RSC Advances

This is an *Accepted Manuscript*, which has been through the Royal Society of Chemistry peer review process and has been accepted for publication.

Accepted Manuscripts are published online shortly after acceptance, before technical editing, formatting and proof reading. Using this free service, authors can make their results available to the community, in citable form, before we publish the edited article. This *Accepted Manuscript* will be replaced by the edited, formatted and paginated article as soon as this is available.

You can find more information about *Accepted Manuscripts* in the Information for Authors.

Please note that technical editing may introduce minor changes to the text and/or graphics, which may alter content. The journal's standard Terms & Conditions and the Ethical guidelines still apply. In no event shall the Royal Society of Chemistry be held responsible for any errors or omissions in this *Accepted Manuscript* or any consequences arising from the use of any information it contains.

ROYAL SOCIETY OF CHEMISTRY

www.rsc.org/advances

Please do not adjust margins

Journal Name

ARTICLE

Lead-free $BaTiO_3$-$Bi(Zn_{2/3}Nb_{1/3})O_3$ weakly coupled relaxor ferroelectric materials for energy storage

Received 00th January 20xx,
Accepted 00th January 20xx

DOI: 10.1039/x0xx00000x

www.rsc.org/

Longwen Wu, Xiaohui Wang*, Longtu Li*

Lead-free (1-x)$BaTiO_3$-x$Bi(Zn_{2/3}Nb_{1/3})O_3$ (x = 0.05-0.20) materials were fabricated via solid-state reactions. Pure perovskite pseudocubic structure is obtained for all compositions. Dielectric measurements reveal an intensified diffusion and relaxor-like characteristics from 5 mol% to 20 mol% $Bi(Zn_{2/3}Nb_{1/3})O_3$. Weakly coupled relaxor behavior is concluded from the exceptionally high activation energies of ~0.20-0.22 eV from the Vogel-Fulcher model for x >= 0.10, which possibly results in the extremely low dielectric nonlinearity and extra slim polarization-electric field loops. An optimal discharged energy density of 0.79 J cm^{-3} with a high energy efficiency of 93.5% is achieved at 131 kV cm^{-1} for x = 0.15, which proves the $BaTiO_3$-$Bi(Zn_{2/3}Nb_{1/3})O_3$ material to be a promising candidate for high energy storage application.

Introduction

Today's advanced power electric and electronic system booming has been forcing the refashioning of energy storage devices[1-5] to meet the development and application of novel pulsed power devices, electric vehicles, wind or solar energy, smart grid, etc.[6-8] Energy storage devices in service or on the way of exploitation cover a wide range, including fuel cells, lithium ion batteries, electrochemical supercapacitor, and electrostatic capacitors,[9, 10] among which the application of electrostatic capacitors with the highest power density is still limited by their relatively low energy storage density. Electrostatic capacitors, normally speaking, consist of two conducting plates or foils separated by a dielectric layer, of which the ultimate energy storage critically relies on the dielectric materials. Generally, dielectric materials under intensive study can be classified into four categories: linear dielectrics, ferroelectrics, antiferroelectrics, and relaxor ferroelectrics.[11, 12] In order to achieve high energy density, principally, high saturation polarization (P_s), low remnant polarization (P_r) and large dielectric breakdown strength (E_B) have to be concurrently achieved.[13] Linear dielectrics including mica,[1] glass,[14-16] paraelectric ceramics[6, 17] and polymers[18] show advantage in their high E_B, while the final energy density fades due to the limitations of small polarization or low permittivity. Ferroelectrics with spontaneous polarization are highly polarizable, but the high P_r , early polarization saturation, moderate E_B and large energy loss stand in the way of the utilization for energy storage devices.[17] Antiferroelectrics, which undergo the ferroelectric to antiferroelectric transition under a certain applied electric field, has very large P_s ; nevertheless, superior energy storage behaviors are only attainable with the break of the restrictions of low temperature stability and modest cycling life expectancy.[19-21] In contrast, relaxor ferroelectrics with slim hysteresis and low P_r which provide high P_s and super energy conversion efficiency are gaining a growing number of interest for the application as high energy density materials with fast discharge ability.[22-27]

Due to the toxicity nature of traditional lead-based relaxor ferroelectrics, such as $Pb(Mg_{1/3}Nb_{2/3})O_3$ (PMN), (PZN) and $Pb(Ni_{1/2}Zr_{1/2})O_3$ (PNZ), researchers are nowadays dedicated to the search of new lead-free alternatives. Environment friendly bismuth (Bi) situated behind lead (Pb) in the periodical table of elements has aroused lots of attentions, due to the fact that the trivalent ion (Bi^{3+}) has a lone pair electronic configuration similar to Pb^{2+}.[28, 29] Bi_2O_3 has been traditionally serving as a sintering aid to improve the microstructure,[30, 31] or as a dopant to tune the electrical properties of ceramics,[32-34] until the innovative study of $0.7BaTiO_3$-$0.3BiScO_3$ as high energy density material by Ogihara, et al.[35] Followingly, promising high energy density was also demonstrated in similar $BaTiO_3$-$Bi(Me)O_3$ (Me symbolizes the trivalent or averagely trivalent metallic ion) ceramic systems, such as $BaTiO_3$-$BiYbO_3$,[36] $BaTiO_3$-$Bi(Mg_{2/3}Nb_{1/3})O_3$,[37] $BaTiO_3$-$Bi(Mg_{1/2}Ti_{1/2})O_3$,[38]etc.

In this work, we report a novel $BaTiO_3$-$Bi(Zn_{2/3}Nb_{1/3})O_3$ ferroelectric relaxor material for energy storage applications. The phase structures and the dielectric behaviors accompanied by the dielectric–temperature dispersion, as well as the relaxor phenomena were thoroughly demonstrated and analyzed. Finally, excellent energy storage density with high energy efficiency was successfully achieved. The possible mechanisms

State Key Laboratory of New Ceramics and Fine Processing, School of Materials Science and Engineering, Tsinghua University, Beijing 100084, P. R. China. Corresponding author E-mail: wxh@mail.tsinghua.edu.cn; llt-dms@mail.tsinghua.edu.cn.*

† Footnotes relating to the title and/or authors should appear here.
Electronic Supplementary Information (ESI) available: [details of any supplementary information available should be included here]. See DOI: 10.1039/x0xx00000x

RSC Advances Accepted Manuscript

Please do not adjust margins

leading to the resulting outstanding performances were also exploited and disscussed.

Experimental

(1-x)$BaTiO_3$-x$Bi(Zn_{2/3}Nb_{1/3})O_3$ (BT-BZN) ceramics with x = 0.05, 0.10, 0.15, 0.20 (0.05BZN, 0.10BZN, 0.15BZN, 0.20BZN) were prepared through conventional solid-state reactions. Analytical grade $BaCO_3$ and TiO_2 as starting powders were purchased from Aladdin Industrial Incorporation (Shanghai, China). Bi_2O_3, ZnO and Nb_2O_5 raw materials were obtained from Sinoparm Chemical Reagent Company (Beijing, China). The raw powders were stoichiometrically weighed, and then ball-milled using zirconia balls for 24 h with isopropanol as media. After drying, the mixed powders were calcined at 850~900 ℃ for 4 h in a closed alumina crucible to prevent the volatilization loss of bismuth oxide. The calcined powders were re-milled, granulated with 5 wt% PVA binder, and uniaxially pressed into pellets with 6 mm in diameter and 0.5~0.6 mm in thickness under the pressure of 2 MPa. The samples were sintered at 1175~1250 ℃ for 2 h in a covered crucible after the burnout of binder at 600 ℃ for 2 h.

The phase structures of the ceramics were determined by X-ray diffraction (XRD; Rigaku 2500, Japan) with Cu K_α radiation (λ = 1.5406 Å) operated at 40 kV and 150 mA. Rietveld refinement method was applied to calculate the lattice parameters of the samples. The microstructures of the sintered ceramic samples were observed using scanning electron microscopy (SEM, Merlin VP Compact, Carl Zeiss, Germany). For electrical measurements, all the sintered samples were polished and coated with silver paste on both sides. Dielectric-temperature response was measured with an Alpha-A impedance analyzer coupled with a temperature controller (Novocontrol Technologies GmbH & Co. KG, Germany) in the frequency range of 100 Hz to 1 MHz under temperatures from -100 to 285 ℃. The direct current (DC) bias properties were measured under the capacitance-voltage (C-V) mode on a power device analyzer/curve tracer (B1505A, Agilent Technologies, USA) at a maximum applied electric field of 30 kV cm^{-1}. The impedance spectra were recorded with an impedance/gain-phase analyser (Solartron ST 1260, USA) at elevated temperatures from 500 ℃ to 600 ℃. The dielectric breakdown strength of the samples was tested in silicon oil at ambient temperature on a voltage withstanding tester (YD2013, Changzhou Yangzi Electronic Co., Ltd, China). Polarization-electric field (*P-E*) hysteresis loops were measured using a TF Analyzer 2000E workstation (Advanced Customized Characterization Technologies, Germany) based on a virtual ground circuit at room temperature and 1 Hz.

Results and discussion

The XRD patterns of BT-BZN ceramics with various BZN content are presented in Figure 1(a). Pervoskite structures with no detectable secondary phases were formed, as evidenced by the strong diffraction peaks pertaining to JCPDS no. 75-0212. No splitting of the (200) peak can be found in Figure 1(b), demonstrating that the BT-BZN ceramics can be indexed as a pseudocubic structure.[39] The XRD patterns are in consistency with those reported by Paterson, et al[40], except for the disparity that secondary phases of higher BZN content were observed in their report, the reason of which is still uncertain. Moreover, with the gradual increase of BZN concentration, the diffraction peaks shown in Figure 1(b) shift towards lower degrees, which is a symbol of the widening the interplanar spacing. To further illustrate this phenomenon, lattice parameters of the samples were calculated and shown in Figure 1(c). Regardless of the slightly smaller radius of Bi^{3+} (1.03 Å < $r(Bi^{3+})$ < 1.61 Å) than Ba^{2+} (1.61 Å) of 12-fold coordination in A-site,[41, 42] the radii of Zn^{2+} (0.74 Å) and Nb^{5+} (0.64 Å) cations are larger than that of the B-site Ti^{4+} (0.605 Å).[43, 44] Both the lattice parameter and unit cell volume were found to become larger with the increase of BZN amount, which demonstrates the domination of the B-site substitution of Zn^{2+} and Nb^{5+} for Ti^{4+} that causes the lattice expansion.[45]

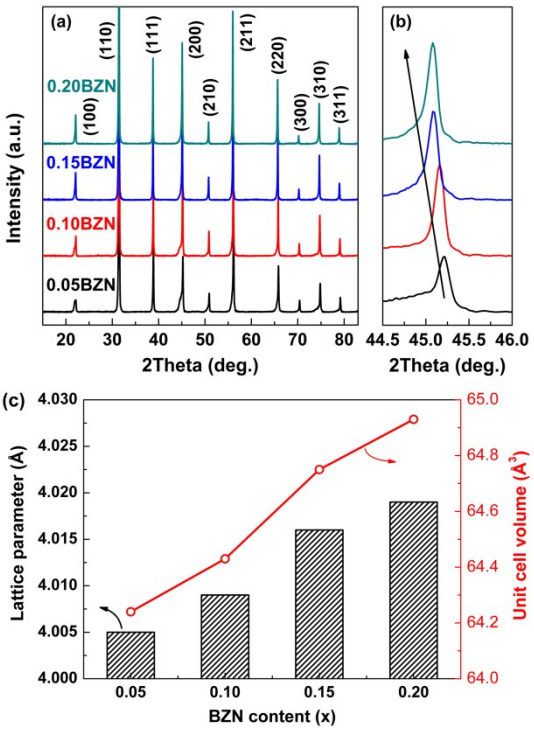

Fig. 1. (a) XRD patterns of the BT-BZN ceramics. (b) Magnification of the patterns in (a) from 44.5° to 46.0°. (c) Lattice parameter and unit cell volume as a function of the content of BZN.

RSC Advances Accepted Manuscript

This journal is © The Royal Society of Chemistry 20xx

Typical morphologies of the thermally etched fractured surfaces of the BT-BZN ceramic samples are displayed in the SEM images (Figure 2). It can be seen that all the four samples are densely sintered as confirmed by the existence of few pores, and the average grain size of the four samples with different BZN concentration shows almost consistently 1~2 μm.

Figure 3 shows the temperature dependence of the real and imaginary parts of dielectric constant of BT-BZN ceramics at increasing frequencies from 100 Hz to 1 MHz. At lower temperatures, the dielectric permittivity peaks shifting towards higher temperature with increasing frequency, known as the frequency dispersion, is found in all the four samples for either the real or the imaginary part of permittivity. With the increase of BZN content from 0.01 to 0.20, this dispersive behavior becomes more prominent, leading to the flattening and broadening of the temperature-dependent permittivity, which is in agreement with the previous report.[40] This interesting phenomenon is generally owing to the emergence of relaxor behavior arising from random fields created by cation disorder that break the development of long-range polar ordering.[46, 47] As a matter of fact, this relaxation behavior is also widely observed in other similar Bi-based ceramic systems.[20, 36, 37, 43-47]

The relaxation behavior can be simply quantified by ΔT_m as:[48]

$$\Delta T_m = T_m(1\,\mathrm{MHz}) - T_m(100\,\mathrm{Hz}) \quad (1)$$

where $T_m(1\,\mathrm{MHz})$ and $T_m(100\,\mathrm{Hz})$ are the temperature dependent dielectric maxima of the real part at frequencies of 1 MHz and 100 Hz, respectively. The calculated results of ΔT_m from Equation (1) for the four samples (listed in Table 1) exhibit an increasing trend with increasing BZN ingredient, which demonstrates an intensified relaxation manner of the BT-BZN ceramics. It is generally acknowledged that in the case of classical first-order displacive ferroelectric phase transition, pure BT shows a sharp peak at the Curie point in the dielectric-temperature response without significant dispersion, which follows the Curie-Weiss law. Nevertheless, in the BT-BZN ceramics, strong frequency dispersion is observed due to ferroelectric relaxation. In this case, a modified empirical model[49, 50] can be applied as Equation (2),

$$\frac{1}{\varepsilon_r} - \frac{1}{\varepsilon_m} = \frac{(T - T_m)^\gamma}{2\varepsilon_m \delta^\gamma} \quad (2)$$

where ε_r is the permittivity, ε_m is the permittivity at T_m, T is the temperature, δ is the diffuseness parameter, and γ is the critical exponent with the value varying from $\gamma = 1$ for a normal ferroelectric to $\gamma = 2$ for an ideal relaxor ferroelectric.[51] The two parameters γ and δ were obtained by fitting the dielectric data at 1 MHz to Equation (2), and

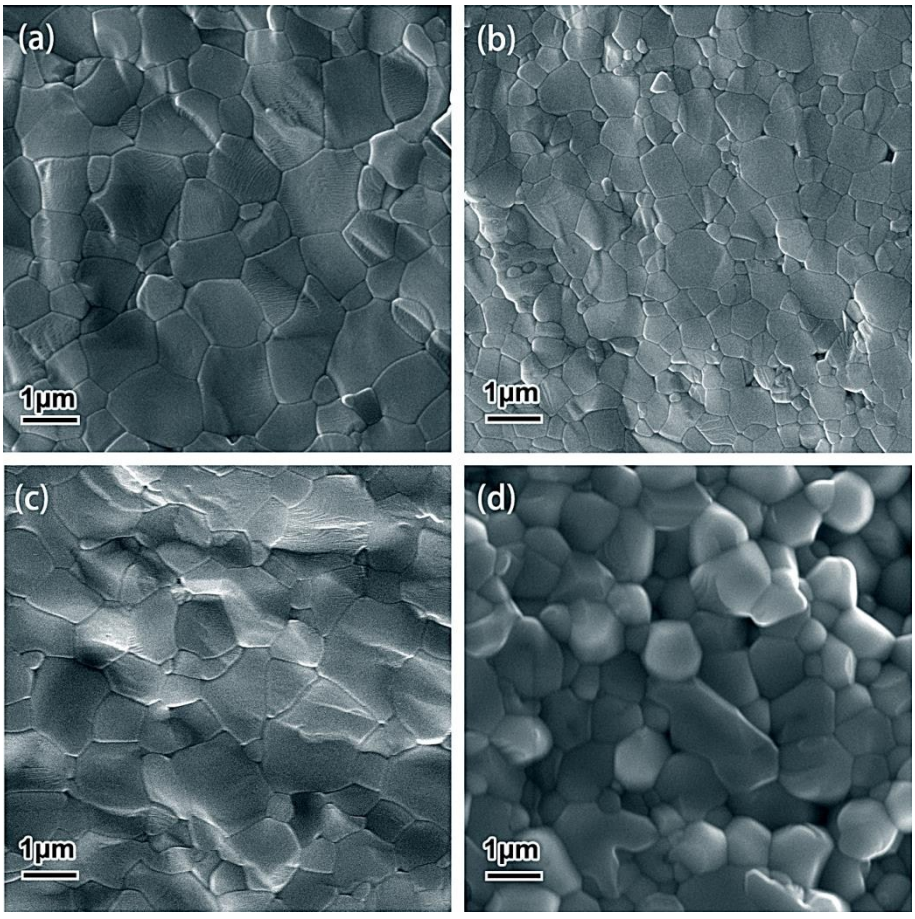

Fig. 2. SEM images for the thermally etched fractured surface of (a) 0.05BZN, (b) 0.10BZN, (c) 0.15BZN and (d) 0.20BZN. The thermal etching temperature was set below ~ 100℃ of the sintering temperature for 1 h.

RSC Advances Accepted Manuscript

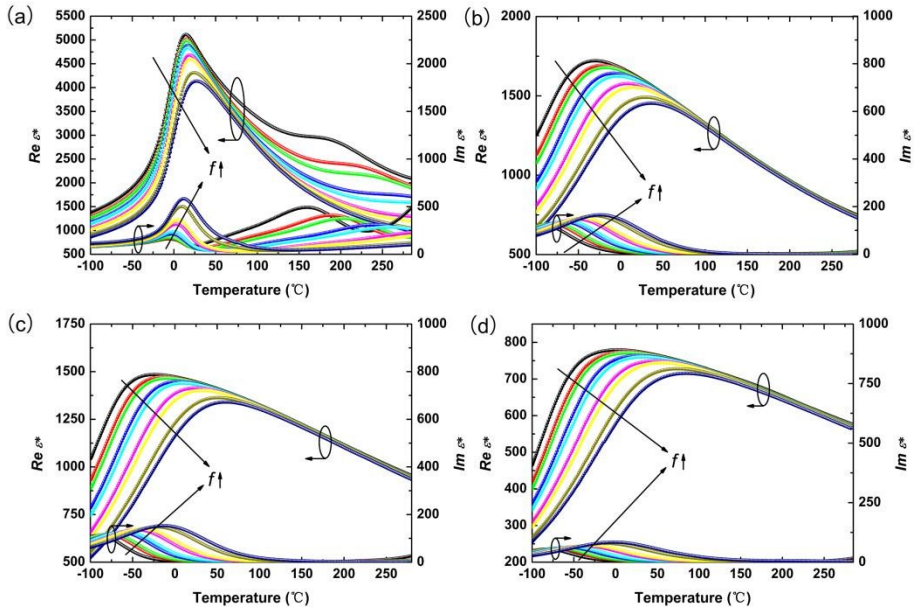

Fig. 3. Temperature dependence of real and imaginary parts of dielectric constant at measuring frequencies from 100 Hz to 1 MHz for (1-x)BT-xBZN: (a) x = 0.05, (b) x = 0.10, (c) x= 0.15, (d) x = 0.20.

good correlations were attained (Figure 4), with results listed in Table 1. The γ values for the four samples were found to be 1.33~1.62, manifesting strong relaxation behavior. More interestingly, the δ values increases from 71 K for x = 0.05 to 551 K for x = 0.20, which indicates that the diffusion intensity is enhanced with the increase of BZN content. Anomalous dispersion peaks with higher values for lower frequencies in the imaginary part and shoulder peaks in the real part at the same temperature range of 0.05BZN sample can be observed at higher temperatures > 150 ℃, which is generally believed to be associated with thermally activated oxygen vacancies, [52, 53] has also been previously reported in $BaTiO_3$ polycrystalline ceramics where grain boundary dominates the capacitive responses.[54] Whereas those anomalous peaks are not distinct for the samples with higher BZN content > 0.05 up to 250 ℃, which can be owing to the compensation for inherent acceptor impurities with further addition of BZN.[55]

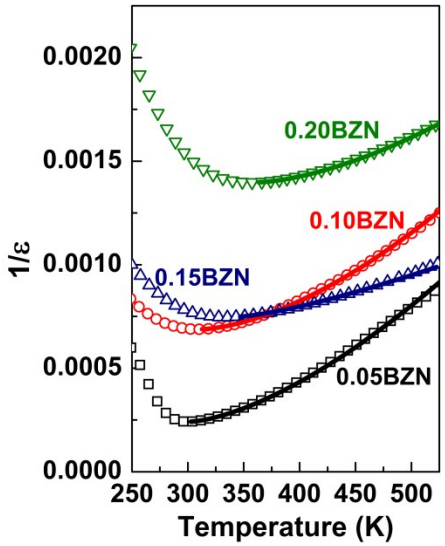

Fig. 4. $1/\varepsilon \sim T$ for the samples of 0.05BZN, 0.10BZN, 0.15BZN and 0.20BZN.

Table 1. Temperature difference of dielectric maxima, critical exponent, diffuseness parameter.

Sample	ΔT_m /K	γ	δ /K
0.05BZN	11.1	1.53	73
0.10BZN	66.4	1.62	156
0.15BZN	93.3	1.33	243
0.20BZN	97.8	1.59	551

RSC Advances Accepted Manuscript

This journal is © The Royal Society of Chemistry 20xx

Please do not adjust margins

The relaxation of relaxor ferroelectrics is a thermally activated process,[56] which is usually believed to be analogous to a spin or dipole glass that the dynamics are only activated above a finite freezing temperature.[57] In this case, the Vogel-Fulcher (V-F) model[58, 59] is applied to characterize this behavior by using the imaginary part of dielectric permittivity. The V-F relationship is expressed in Equation (3) as,

$$f = f_0 \exp\left[-E_a / k_B \left(T_{\max} - T_f\right)\right] \quad (3)$$

where f is the probing frequency, f_0 is the Debye frequency related to the attempt jump, E_a is the activation energy of the relaxation process, k_B denotes the Boltzmann's constant, $T_{\max}$ is the temperature of the imaginary permittivity maximum, and T_f is the freezing temperature. Nonlinear fitting of the VF model was conducted for the four samples, and good correlations were achieved. The fitting results with the obtained parameters are shown in Figure 5(a)-(d), respectively. The activation energy for the 0.05BZN sample is 0.029 ± 0.004 eV, which is similar to classical relaxor ferroelectrics, such as PMN[60] and PZN[61]. Attentions should be specially focused on the samples with BZN compositions > 0.05 that the activation energies ($E_a \approx 0.20 - 0.22\,\text{eV}$) are about one order higher than the 0.05BZN sample of classical relaxor ferroelectric behavior. This unusual phenomenon is also observed other $BaTiO_3$-$BiMeO_3$ systems, for instance, $BaTiO_3$-$BiScO_3$ ($E_a \approx 0.24 - 0.26\,\text{eV}$),[62] $BaTiO_3$-$Bi(Mg_{1/2}Ti_{1/2})O_3$ ($E_a \approx 0.17 - 0.22\,\text{eV}$),[63] $BaTiO_3$-$Bi(Zn_{1/2}Ti_{1/2})O_3$ ($E_a \approx 0.16 - 0.25\,\text{eV}$),[64] and $BaTiO_3$-$Bi(Zn_{1/2}Ti_{1/2})O_3$-$BiScO_3$ ($E_a \approx 0.37 - 0.50\,\text{eV}$).[43] High activation energies imply that it is difficult to obtain long-range dipole alignment under field-cooled conditions, and the polar clusters are isolated and frustrated, leading to only weakly coupling between neighboring clusters. Macroscopic switching of the polarization of the so-called "weakly coupled relaxor" is enabled at low temperatures with high fields.[62] This behavior is extremely beneficial for energy storage, because it is usually associated with low dielectric nonlinearity (or high polarization saturation field) and slim hysteresis (or low energy loss), as will be discussed hereinafter in this work.

Energy-storage capacitors deliver energy by first charging from zero electric field to an efficiently high field, and then discharging backwards. As the energy storage behavior of the capacitors is closely related to the permittivity, the dielectric constant variation with applied electric field, known as the dielectric nonlinearity, is conducted by DC-bias performances under the C-V mode at ambient temperature and 10 KHz. As shown in Figure 6(a)-(d), except for the size difference of the enclosed area, all the dielectric constants as functions of applied electric field for the four samples display butterfly-like loops due to the energy loss during the process of charging and discharging, and to note, the larger area for the 0.20BZN sample may be also in part originated from the less well sintered microstructure in Figure 2d. It can also be noticed that

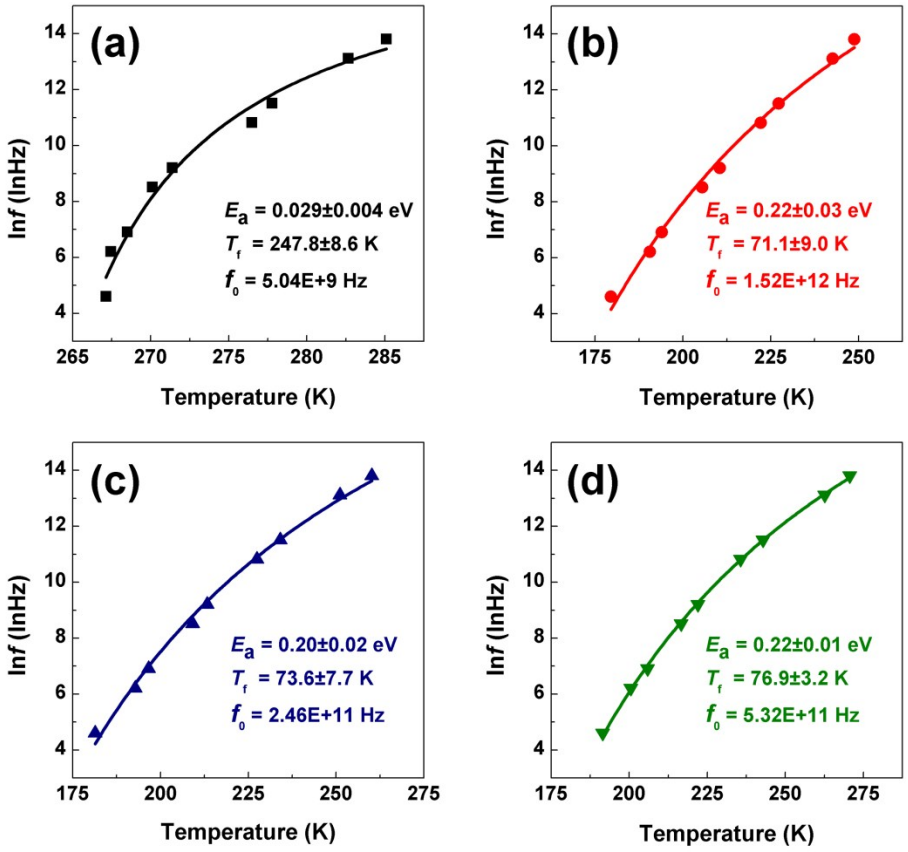

Fig. 5. Vogel-Fulcher fit for BT-BZN ceramics with various BZN content: (a) 0.05BZN, (b) 0.10BZN, (c) 0.15BZN, (d) 0.20BZN. The insets show the fitting parameter values.

RSC Advances Accepted Manuscript

the dielectric constant under no bias field decreases with increasing BZN additive, which is in correspondence to the dielectric response shown in Figure 3 and could be originated from the frustration of long-range polarization ordering with the addition of BZN.[37] Moreover, for all the four samples with different compositions, the dielectric constant decreases to some extent with the elevation of the applied electric field. To better examine this behavior, the relative permittivity changes are evaluated, as defined in Equation (4),

$$\text{Permittivity Change} = \frac{\varepsilon_r(E) - \varepsilon_r(0)}{\varepsilon_r(0)} \times 100\% \quad (4)$$

where $\varepsilon_r(0)$ and $\varepsilon_r(E)$ are the relative permittivity under an applied bias field of zero and E, respectively. Figure 6(e) exhibits the electric field dependence of the permittivity change of the BT-BZN ceramics with various compositions. At an electric field of 30 kV cm^{-1}, the permittivity changes for the 0.05BZN, 0.10BZN, 0.15BZN and 0.20BZN samples are -60.0%, -6.7%, -2.4%, -1.6%, respectively, showing a declining trend with increasing content of BZN. The 0.05BZN sample suffers from a dramatic discrepancy compared to the other three samples, which may be arising from the activation energy difference that distinguishes it as a strongly coupled classical ferroelectic relaxor from the other three samples of weakly coupled relaxor behavior.

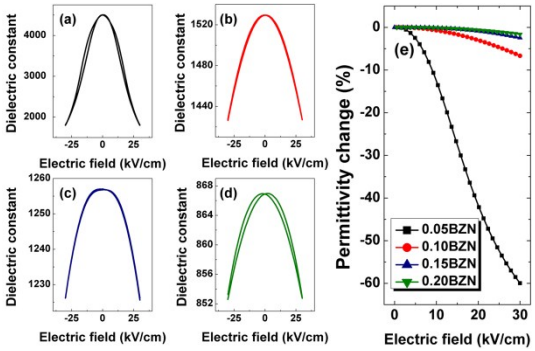

Fig. 6. Dielectric constant as a function of applied electric field: (a) 0.05BZN, (b) 0.10BZN, (c) 0.15BZN, and (d) 0.20BZN. (e) Permittivity change versus electric field for the BT-BZN ceramics with various BZN content.

The resistivity performances of the BT-BZN ceramics were examined by impedance spectroscopy, which is regarded as a powerful tool to separate the contribution of grain, grain boundary, interfaces, electrodes, etc.[64] The impedance spectroscopy was conducted at activation temperatures from 500 ℃ - 600 ℃. The black dots of Figure 7(a)-(d) display the Z''-Z' plots measured at 550 ℃ for the BT-BZN ceramics where the semicircles are suppressed and overlapped. Therefore, the impedance data were deconvoluted with two *R*-CPE[65] (Figure S1) responses of grain and grain boundary, where CPE is constant phase element. *R*, CPE-*T* and a relaxation distribution parameter CPE-*P* can be evaluated (R_g, CPE_g-*T*, CPE_g-*P*, R_{gb}, CEP_{gb}-*T*, CPE_{gb}-*P*). The equivalent capacitance values of the

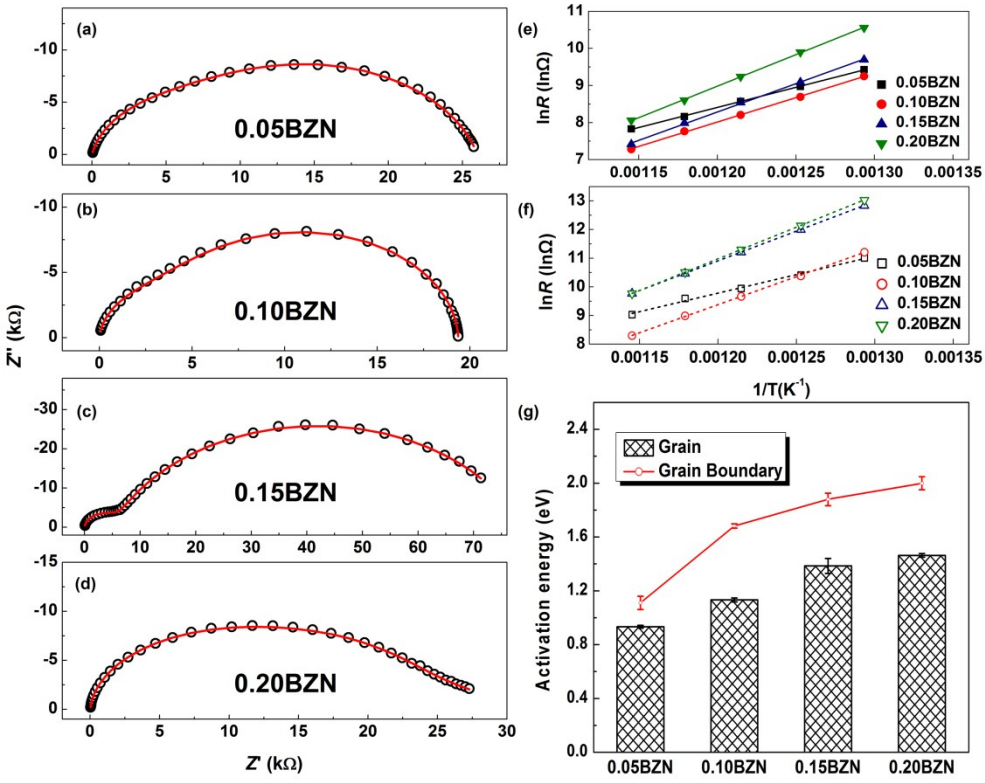

Fig. 7. Complex plane plot of Z''-Z' for measured (black circles) and fitted (red line) data at 550 ℃: (a) 0.05BZN, (b) 0.10BZN, (c) 0.15BZN, (d) 0.20BZN. Arrhenius fit to the resistance data of the grain (e) and grain boundary (f) for various BT-BZN ceramics. (g) Activation energy of grain and grain boundary for ceramics with different BZN content.

RSC Advances Accepted Manuscript

This journal is © The Royal Society of Chemistry 20xx

grain (C_g) and grain boundary (C_{gb}) can be calculated via $C = (R*\text{CPE-}T)^{1/\text{CPE-}P}/R$.[66] Nonlinear least square (NLLS) fittings were applied to the impedance data with corresponding electric parameters listed in Table S1. For all the samples, quite reasonable values of both the C_g and C_{gb} ranging 10^{-10} - 10^{-9} F are achieved.[67] Good correlations are attained, as shown in the small discrepancy between the experimental and fitted data in Figure 7(a)-(d).

The reciprocal capacitance values of grain and grain boundary versus temperature from the NLLS fittings were shown in Figure S2(a) and Figure S2(b), respectively. For all the samples, the C_g regenerates the Cure-Weiss behavior[68] well with extrapolated Curie temperature of 95℃ - 110℃. The calculated slopes are 169000 ℃ - 267000 ℃, in good consistency with the Curie constant of bulk $BaTiO_3$ of the order of ~ 150000 ℃.[69] The behavior of C_{gb} is similar to the constriction boundary model,[68] where the reciprocal of C_{gb} are roughly constant or slightly increase with the elevation of temperature. These results confirm the good reasonability of the evaluated resistance and capacitance values of grain and grain boundary from the as-adopted equivalent circuit model.

The resistance of the grain and the grain boundary can be viewed as thermally activated process, and therefore, the resistance data obtained from the fittings for the grain and grain boundary are separately considered by the Arrhenius relationship, as depicted in Equation (5),

$$R = R_0 \exp\left(\frac{E_a}{kT}\right) \quad (5)$$

where R is the resistance, R_0 is the pre-exponential factor, E_a is the resistance activation energy, k is the Boltzmann's constant, and T here is the temperature in kelvin. By change Equation (5) into the form of $\ln R \sim 1/T$, linear regression was applied with good results obtained, as shown in Figure 7(e) for the grain, and Figure 7(f) for the grain boundary, respectively. The acquired E_a of the grain boundaries are higher than those of the grains for all the BT-BZN compositions, indicating that the major resistivity contribution at elevated temperatures should be owing to the grain boundaries. In addition, E_a of both the grain and grain boundary become larger with the increase of BZN content, demonstrating that the insulation ability is enhanced with increasing amount of BZN.

The dielectric breakdown strength is one of the key characteristics benchmarking the performance of high power or high energy-density dielectrics. Weibull distribution, which is widely applied in the analysis of failure or breakdown, is adopted here for the evaluation of the breakdown strength data obtained at room temperature. The two-parameter cumulative distribution function is adopted as defined in Equation (6)

$$P = 1 - \exp\left[-\left(\frac{E}{\alpha}\right)^{\beta}\right] \quad (6)$$

where P is the cumulative probability of failure, α is a scale parameter characterizing the breakdown strength, β is a shape parameter indicating the dispersion of the data, and E is the critical electric field above which breakdown occurs. The breakdown strength data are ranked in an ascending order and the values of P are estimated as Equation (7)

$$P = \frac{j}{N+1} \quad (7)$$

where j is the rank and N is the total number of samples. The Weibull moduli α and β were then determined through linear regression of $\ln\left(-\ln\left(1-P\right)\right) \sim \ln E$, with results manifested in Figure 8. It can be seen that good correlations were reached, demonstrating good applicability of the two-parameter model, and that the shape parameters β with values more than three are obtained for all the BT-BZN ceramics, demonstrating high reliability of the Weibull analysis.[70] Generally, declined permittivity is associated with higher breakdown strength.[71] However, reduced breakdown strength is obtained for the 0.20BZN sample, which may be owing to its less well sintered microstructure. In this case, the characteristic breakdown strength α reaches the maximum with the value of 262 kV cm^{-1} for the 0.15BZN ceramics, which means that under the testing conditions, the 0.15BZN ceramics are the most breakdown resistant.

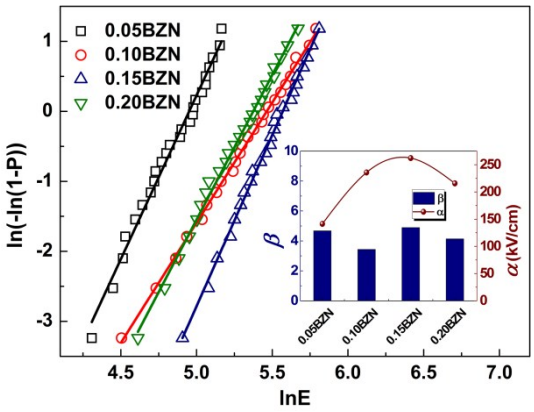

Fig. 8. Weibull fit of the breakdown strength data for various BT-BZN ceramics. The inset shows the obtained α and β values, respectively.

The energy storage behaviors of the BT-BZN ceramics were investigated via the *P-E* loops. Figure 9 shows the *P-E* loops of the ceramics with different BZN concentrations measured at a maximum applied electric field of 60 kV cm^{-1}. Because of the relaxor behavior mentioned hereinbefore, square *P-E* loops with large remnant polarization and high coercive field which is a fingerprint of ferroelectrics are not observed for all samples. In the BT-BZN relaxor ceramics, due to the incorporation of BZN dopant into the BT host, the long-range dipolar interaction is disrupted and local isolated polar nanoregions (PNRs) are formed resulting from the composition fluctuation and charge difference. Because the PNRs are of smaller characteristic size than the ordinary ferroelectric domains or macroscopic domains, the aligning and

RSC Advances Accepted Manuscript

backswitching of the domains become easier manifested in that they are more apt to the applied electric field, which often leads to slimmer hysteresis loops.[72] More interestingly, one can observe that the BT-BZN ceramics with higher BZN content ($x \geq 0.10$) exhibit almost linear *P-E* loops with neglectable hysteresis. The $P_m - P_r$ values are almost identical to P_m (refer to the circled area in the inset of Figure 9), which is technologically meaningful because large $P_m - P_r$ values are often favorable for high discharged energy density.[73] The underpinning reason why there exists such a big disparity should be the weakly coupled behavior of these ceramics, as analyzed hereinbefore that domain coupling which can only occur under low temperature and high electric field is weaker compared to classical ferroelectric relaxor of the BT-BZN ceramic with x = 0.05.

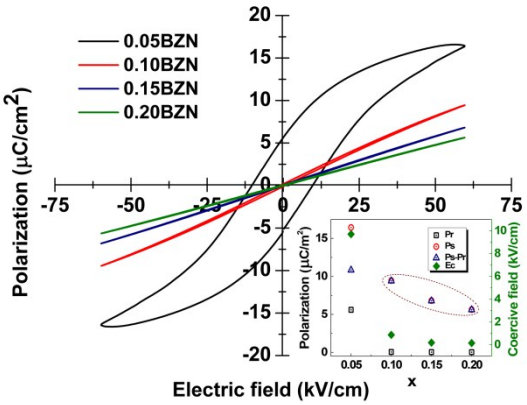

Fig 9. *P-E* loops for various BT-BZN ceramics. The inset shows the composition dependent Pr, Es, Ps-Pr and Ec.

The BT-BZN ceramics are meritorious for energy storage as concluded from their *P-E* relationships. Due to hysteresis or conduction loss, the charge and discharge paths are not coincident, for which both the energy storage density and energy efficiency should be taken into account in the view of practical applications. The energy storage density (W_{stor}) and energy efficiency (η) can be evaluated by Equation (8) and Equation (9), respectively:

$$W_{stor} = \int_{P_r}^{P_m} E \, dP \qquad (8)$$

$$\eta = \frac{W_{stor}}{W_{stor} + W_{loss}} \times 100\% \qquad (9)$$

where P_r is the remnant polarization, P_m is the maximum polarization at the maximum applied electric field, W_{loss} is the energy loss density due to domain reorientation and leakage conduction. Graphically, W_{stor} is equal to the area enclosed by the discharge polarization curve and the y-axis, and correspondingly, W_{loss} is the enclosed area of the charge and discharge polarization curve. In the calculations, all the integrations were taken numerically using the trapezoidal method. The as-calculated charged and discharged density, as well as the energy efficiency is shown in Figure 10. At the same applied electric field, the 0.05BZN ceramic exhibits the highest charged energy density due to its high permittivity and polarization (Figure 10a). Nevertheless, this advantage is offset by its high energy loss, leading to a small discharged energy density of 0.37 J cm^{-3} at 100 kV cm^{-1} (Figure 10b) and a low efficiency < 50% (Figure 10c), which indicates that a high polarization does not necessarily result in high energy storage unless the energy loss is concurrently maintained low. This conclusion holds particularly true for the high energy storage behaviors of the BT-BZN ceramics with $x \geq 0.10$ whose permittivity and polarization are moderate, as compared from the Figure 10(a)-(c). It is worth noting that energy efficiency of these ceramics reaches as high as more than 90% at all applied electric fields (see the circled area in Figure 10c), which may be originated from the easy domain backswitching associated with their weakly coupled behaviors, and the low leakage conduction as confirmed from the high activation energies of impedance study in Figure 7. Of the four BT-BZN ceramics, the optimal discharged density of 0.79 J cm^{-3} with a high efficiency of 93.5% is achieved at an electric field of 131 kV cm^{-1} for the ceramic with x = 0.15. It is anticipated that the energy density may be further enhanced if the breakdown strength is improved through, i.e., densification[74, 75] or coating with breakdown-resistant materials,[76] due to the fact of the polarization unsaturation at the experimental breakdown field.

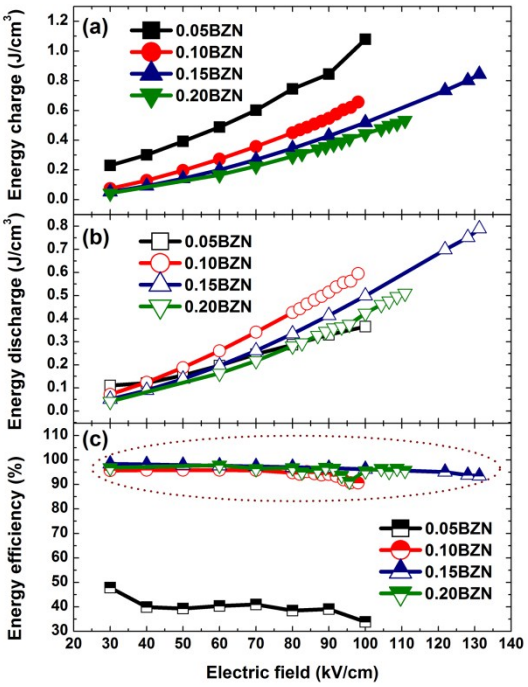

Fig. 10. (a) Charged energy density, (b) discharged energy density, and (c) energy efficiency versus applied electric field of the BT-BZN ceramics.

RSC Advances Accepted Manuscript

This journal is © The Royal Society of Chemistry 20xx

Conclusions

In summary, the (1-x)$BaTiO_3$-x$Bi(Zn_{2/3}Nb_{1/3})O_3$ (x = 0.05-0.20) ceramics were successfully synthesized via a conventional solid-state method. Pure perovskite pseudocubic structure with gradually enlarged lattice parameters is obtained by XRD patterns. With the increase of BZN content, dielectric-temperature responses are becoming highly dispersive, as evidenced by the rather broadened and flattened permittivity peaks, which is further verified by the increase of δ values obtained from a modified Curie-Weiss law. Extremely low dielectric nonlinearity and super slim P-E loops with neglectably small enclosed area are observed for ceramics with $x \geq 0.10$, the possible origin of which is analyzed to be the weakly coupled relaxor behavior as confirmed from the unusually high E_a ~0.20-0.22 eV in the V-F fittings. Finally, an optimal W_{stor} of 0.79 J cm^{-3} with η of 93.5% is achieved at 131 kV cm^{-1} for the ceramic with x = 0.15, which demonstrates that the BT-BZN bulk ceramics are promising candidates for high energy storage applications.

Acknowledgements

The work was supported by Ministry of Sciences and Technology of China through National Basic Research Program of China (973 Program 2015CB654604), National Natural Science Foundation of China for Creative Research Groups (Grant No.51221291), National Natural Science Foundation of China (Grant No. 51272123), and also supported by CBMI Construction Co., Ltd.

Notes and references

1 W. J. Sarjeant, I. W. Clelland and R. A. Price, *Proc. IEEE*, 2001, **89**, 846-855.
2 Q. Li, L. Chen, M. R. Gadinski, S. Zhang, G. Zhang, H. Li, A. Haque, L. Q. Chen, T. Jackson and Q. Wang, *Nature*, 2015, **523**, 576-579.
3 F. X. Guan, L. Y. Yang, J. Wang, B. Guan, K. Han, Q. Wang and L. Zhu, *Adv. Funct. Mater.*, 2011, **21**, 3176-3188.
4 S. A. Sherrill, P. Banerjee, G. W. Rubloff and S. B. Lee, *Phys. Chem. Chem. Phys.*, 2011, **13**, 20714-20723.
5 P. Barber, S. Balasubramanian, Y. Anguchamy, S. Gong, A. Wibowo, H. Gao, H. J. Ploehn and H.-C. zur Loye, *Materials*, 2009, **2**, 1697-1733.
6 H. Lee, J. R. Kim, M. J. Lanagan, S. Trolier-McKinstry and C. A. Randall, *J. Am. Ceram. Soc.*, 2013, **96**, 1209-1213.
7 P. H. Hu, Y. Shen, Y. H. Guan, X. H. Zhang, Y. H. Lin, Q. M. Zhang and C. W. Nan, *Adv. Funct. Mater.*, 2014, **24**, 3172-3178.
8 R. W. Johnson, J. L. Evans, P. Jacobsen, J. R. Thompson and M. Christopher, *IEEE Trans. Electron. Packag. Manuf.*, 2004, **27**, 164-176.
9 I. Hadjipaschalis, A. Poullikkas and V. Efthimiou, *Renew. Sust. Energ. Rev.*, 2009, **13**, 1513-1522.
10 X. Hao, *J. Adv. Dielectr.*, 2013, **3**, 1330001.
11 I. Burn and D. M. Smyth, *J. Mater. Sci.*, 1972, **7**, 339-&.
12 N. Ortega, A. Kumar, J. Scott, D. B. Chrisey, M. Tomazawa, S. Kumari, D. Diestra and R. Katiyar, *J. Phys.: Condens. Matter*, 2012, **24**, 445901.
13 Z. Xie, B. Peng, J. Zhang, X. Zhang, Z. Yue and L. Li, *J. Am. Ceram. Soc.*, 2015, **98**, 2968-2971.
14 M. P. Manoharan, C. Zou, E. Furman, N. Zhang, D. I. Kushner, S. Zhang, T. Murata and M. T. Lanagan, *Energy Technol.*, 2013, **1**, 313-318.
15 W. Zhang, S. Xue, S. Liu, J. Wang, B. Shen and J. Zhai, *J. Alloys Compd.*, 2014, **617**, 740-745.
16 L. Tang, W. Wang, B. Shen, J. Zhai and L. Kong, *J. Electron. Mater.*, 2015, **44**, 227-234.
17 D. P. Shay, N. J. Podraza, N. J. Donnelly and C. A. Randall, *J. Am. Ceram. Soc.*, 2012, **95**, 1348-1355.
18 M. Rabuffi and G. Picci, *IEEE Trans. Plasma Sci.*, 2002, **30**, 1939-1942.
19 X. H. Hao, Y. Wang, L. Zhang, L. W. Zhang and S. L. An, *Appl. Phys. Lett.*, 2013, **102**, 4.
20 J. Hao, Z. Xu, R. Chu, W. Li, D. Juan and F. Peng, *Solid State Commun.*, 2015, **204**, 19-22.
21 Q. Zhang, X. Liu, Y. Zhang, X. Song, J. Zhu, I. Baturin and J. Chen, *Ceram. Int.*, 2015, **41**, 3030-3035.
22 H. Zhu, S. Pruvost, P. J. Cottinet and D. Guyomar, *Appl. Phys. Lett.*, 2011, **98**, 3.
23 X. H. Hao, Y. Wang, J. C. Yang, S. L. An and J. B. Xu, *J. Appl. Phys.*, 2012, **112**, 6.
24 L. Zhu and Q. Wang, *Macromolecules*, 2012, **45**, 2937-2954.
25 Y. Y. Liu, X. H. Hao and S. L. An, *J. Appl. Phys.*, 2013, **114**, 6.
26 L. Zhang and X. H. Hao, *J. Alloys Compd.*, 2014, **586**, 674-678.
27 N. Kumar, A. Ionin, T. Ansell, S. Kwon, W. Hackenberger and D. Cann, *Appl. Phys. Lett.*, 2015, **106**, 252901.
28 A. Simon, J. Ravez and M. Maglione, *Solid State Sci.*, 2005, **7**, 925-930.
29 J. Zhao, H. Du, S. Qu, J. Wang, H. Zhang, Y. Yang and Z. Xu, *J. Alloys Compd.*, 2011, **509**, 3537-3540.
30 V. Gil, J. Tartaj, C. Moure and P. Durán, *J. Eur. Ceram. Soc.*, 2006, **26**, 3161-3171.
31 S. Le, J. Zhang, X. Zhu, J. Zhai and K. Sun, *J. Power Sources*, 2013, **232**, 219-223.
32 C. Ang, Z. Yu, J. Hemberger, P. Lunkenheimer and A. Loidl, *Phys. Rev. B*, 1999, **59**, 6665-6669.
33 H. Wang and Y.-M. Chiang, *J. Am. Ceram. Soc.*, 1998, **81**, 89-96.
34 Y. Noguchi, I. Miwa, Y. Goshima and M. Miyayama, *Jpn. J. Appl. Phys.*, 2000, **39**, L1259-L1262.
35 H. Ogihara, C. A. Randall and S. Trolier-McKinstry, *J. Am. Ceram. Soc.*, 2009, **92**, 1719-1724.
36 Z. Shen, X. Wang, B. Luo and L. Li, *J. Mater. Chem. A*, 2015, **3**, 18146-18153.
37 T. Wang, L. Jin, C. Li, Q. Hu and X. Wei, *J. Am. Ceram. Soc.*, 2014, **98**, 559-566.
38 Q. Hu, L. Jin, T. Wang, C. Li, Z. Xing and X. Wei, *J. Alloys Compd.*, 2015, **640**, 416-420.
39 A. Bootchanont, N. Triamnak, S. Rujirawat, R. Yimnirun, D. P. Cann, R. Guo and A. Bhalla, *Ceram. Int.*, 2014, **40**, 14555-14562.
40 A. Paterson, H. T. Wong, Z. Liu, W. Ren and Z.-G. Ye, *Ceram. Int.*, 2015, **41**, S57-S62.
41 R. Shannon, *Acta Crystallogr. Sect. A*, 1976, **32**, 751-767.

RSC Advances Accepted Manuscript

42 Q. Zhang, Z. Li, F. Li and Z. Xu, *J. Am. Ceram. Soc.*, 2011, **94**, 4335-4339.
43 N. Raengthon, T. Sebastian, D. Cumming, I. M. Reaney, D. P. Cann and J. Roedel, *J. Am. Ceram. Soc.*, 2012, **95**, 3554-3561.
44 H. Cheng, H. Du, W. Zhou, D. Zhu, F. Luo and B. Xu, *J. Am. Ceram. Soc.*, 2013, **96**, 833-837.
45 D. Ma, X. Chen, G. Huang, J. Chen, H. Zhou and L. Fang, *Ceram. Int.*, 2015, **41**, 7157-7161.
46 T. Strathdee, L. Luisman, A. Feteira and K. Reichmann, *J. Am. Ceram. Soc.*, 2011, **94**, 2292-2295.
47 X. Huang, H. Hao, S. Zhang, H. Liu, W. Zhang, Q. Xu and M. Cao, *J. Am. Ceram. Soc.*, 2014, **97**, 1797-1801.
48 C. Lei, A. A. Bokov and Z. G. Ye, *J. Appl. Phys.*, 2007, **101**, 084105.
49 G. A. Smolenskii, *J. Phys. Soc. Jpn*, 1970, **28(Suppl.)**, 26-37.
50 V. V. Kirillov and V. A. Isupov, *Ferroelectrics*, 1973, **5**, 3-9.
51 K. Uchino and S. Nomura, *Ferroelectrics*, 1982, **44**, 55-61.
52 B. S. Kang, S. K. Choi and C. H. Park, *J. Appl. Phys.*, 2003, **94**, 1904.
53 S. K. Choi, B. S. Kang, Y. W. Cho and Y. M. Vysochanskii, *J. Electroceram.*, 2004, **13**, 493-502.
54 L. M. Nunes, E. Antonelli, M. I. B. Bernardi, T. O. Oladeinde, J. A. S. Caceres and J. C. M'Peko, *Mater. Res. Bull.*, 2011, **46**, 136-139.
55 N. Kumar, D. P. Cann and D. C. Lupascu, *J. Am. Ceram. Soc.*, 2015, **98**, 2548-2555.
56 H. Y. Guo, C. Lei and Z.-G. Ye, *Appl. Phys. Lett.*, 2008, **92**, 172901.
57 S. S. N. Bharadwaja, J. R. Kim, H. Ogihara, L. E. Cross, S. Trolier-McKinstry and C. A. Randall, *Phys. Rev. B*, 2011, **83**.
58 H. Vogel, *Phys. Z.*, 1921, **22**, 645-646.
59 G. S. Fulcher, *J. Am. Ceram. Soc.*, 1925, **8**, 339-355.
60 D. Viehland, S. J. Jang, L. E. Cross and M. Wuttig, *J. Appl. Phys.*, 1990, **68**, 2916-2921.
61 Y. H. Bing, A. A. Bokov, Z. G. Ye, B. Noheda and G. Shirane, *J. Phys.: Condens. Matter*, 2005, **17**, 2493.
62 H. Ogihara, C. A. Randall and S. Trolier-McKinstry, *J. Am. Ceram. Soc.*, 2009, **92**, 110-118.
63 D. H. Choi, A. Baker, M. Lanagan, S. Trolier-McKinstry and C. Randall, *J. Am. Ceram. Soc.*, 2013, **96**, 2197-2202.
64 N. Raengthon and D. P. Cann, *J. Am. Ceram. Soc.*, 2012, **95**, 1604-1612.
65 S.-H. Yoon, C. A. Randall and K.-H. Hur, *J. Appl. Phys.*, 2010, **107**, 103721.
66 S.-H. Yoon, C. A. Randall and K.-H. Hur, *J. Am. Ceram. Soc.*, 2009, **92**, 1758-1765.
67 J. T. S. Irvine, D. C. Sinclair and A. R. West, *Adv. Mater.*, 1990, **2**, 132-138.
68 N. Hirose and A. R. West, *J. Am. Ceram. Soc.*, 1996, **79**, 1633-1641.
69 J. C. Slater, *Phys. Rev.*, 1950, **78**, 748-761.
70 A. R. Blythe and D. Bloor, *Electrical properties of polymers*, Cambridge University Press, 2005.
71 J. McPherson, J.-Y. Kim, A. Shanware and H. Mogul, *Appl. Phys. Lett.*, 2003, **82**, 2121-2123.
72 L. Jin, F. Li and S. Zhang, *J. Am. Ceram. Soc.*, 2014, **97**, 1-27.
73 D. Zheng, R. Zuo, D. Zhang and Y. Li, *J. Am. Ceram. Soc.*, 2015, **98**, 2692-2695.
74 Y. H. Huang, Y. J. Wu, W. J. Qiu, J. Li and X. M. Chen, *J. Eur. Ceram. Soc.*, 2015, **35**, 1469-1476.
75 J. X. Ding, Y. F. Liu, Y. N. Lu, H. Qian, H. Gao, H. Chen and C. J. Ma, *Mater. Lett.*, 2014, **114**, 107-110.
76 B. Liu, X. Wang, Q. Zhao and L. Li, *J. Am. Ceram. Soc.*, 2015, **98**, 2641-2646.

RSC Advances Accepted Manuscript

This journal is © The Royal Society of Chemistry 20xx

Please do not adjust margins

High energy density $BaTiO_3$-$Bi(Zn_{2/3}Nb_{1/3})O_3$ materials with concurrently high energy efficiency

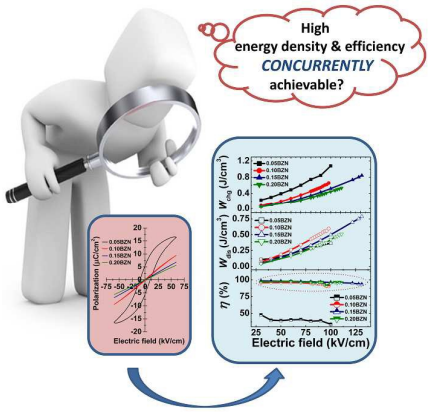

RSC Advances Accepted Manuscript